

# Simulation of Eddy Current Losses in Twisted Wires

Tamás Bakondi<sup>1\*</sup>

<sup>1</sup> Department of Broadband Infocommunications and Electromagnetic Theory, Faculty of Electrical Engineering and Informatics, Budapest University of Technology and Economics, Műegyetem rkp. 3., H-1111 Budapest, Hungary

\* Corresponding author, e-mail: [bakondi.tamas@edu.bme.hu](mailto:bakondi.tamas@edu.bme.hu)

Received: 13 June 2023, Accepted: 04 July 2023, Published online: 08 January 2024

## Abstract

Twisted wires made of insulated strands, known as stranded conductors or litz wires, are used in various areas where the eddy current loss within the wire needs to be reduced. These areas include induction heating, resonance-based wireless energy transfer, and certain radio frequency devices. Some litz wires consist of thousands of individual conductor strands that are twisted together in multiple stages, creating a hierarchical bundle structure. Computer simulations (typically using finite element analysis) are used in the optimal design of the bundle structure. However, detailed three-dimensional models are computationally demanding. In this work, a two-dimensional finite element model was presented for simulating the eddy current loss in cables made of twisted wires. The key element of the model is considering the bundle structure (generally referred to as 3D configuration conditions) within the cross-sectional model domain. The accuracy of the proposed model is tested against 3D finite element simulations. The new method is shown to be accurate, and its computational cost is by orders of magnitude lower than that of 3D models.

## Keywords

litz wire, finite element method, eddy current, two-dimensional model

## 1 Introduction

Litz wires are special types of wires that consist of multiple isolated thin elemental conductors, which are connected at their ends. These strands are twisted together, and the resulting bundles are further twisted or braided into larger bundles, creating a multi-level, complex wire structure. In high-frequency devices that operate at frequencies up to a few hundred kilohertz, litz wires are commonly used because their eddy current losses are significantly lower than those of solid conductors [1]. This makes it possible to reduce the size and electromagnetic interference of the devices. For example, these cables are used to make induction heating coils, as well as in switch-mode power supplies and wireless energy transfer systems based on coupled resonators, where minimizing losses is critically important [2]. The components of eddy current losses strongly depend on the structure of the wire, i.e., on the way the strands are bundled and twisted or braided together. Simulating the loss mechanism helps to optimize wire construction, which is why several researchers have studied the behavior of litz wires and the optimal construction methods for their implementation [3]. There are several techniques used to model litz wires, such as finite element-based methods, integral equation-based methods [4], or the PEEC (Partial Element

Equivalent Circuit) method [5]. Additionally, various homogenization techniques exist [6].

In this article, we present an approach based on two-dimensional (2D) Finite Element Method (FEM). Several researchers previously discussed two-dimensional modeling, and it has a long history [7, 8]. While FEM can be performed in three dimensions (3D), modeling in 3D with the necessary level of accuracy is extremely resource-intensive.

Modeling complex wire constructions consisting of thousands of elementary conductor strands is extremely resource-intensive. Even a single longitudinal period of a twisted cable can only be covered with a very large number of elements. The computational resources required can be effectively reduced by using two-dimensional cross-sectional modelling. With 2D modeling, the computing time of 3D models can be reduced from several hours to just a few tens of seconds. However, some of the physical phenomena, such as the effect of twisting and braiding or voltage and current constraints (see Section 2), must be taken into account. The key to two-dimensional modeling, and also the aim of this work, is to properly implement these constraints. This article builds upon the procedures presented in the recent paper [9].

## 2 Theory

In the case of untwisted conductors, the most obvious way to simplify calculations would be to take advantage of translational symmetry and model only one specific cross-section. In the case of twisted or braided conductors, these symmetries do not strictly hold. However, if the movement of the strands along the length is relatively slow (e.g., the twisting period of a twisted wire is much larger than its diameter), then in practical terms, we can talk about a constant cross-section and quasi-two-dimensional models resulting from this. Let us first consider Fig. 1, in which a litz wire is shown connected to generators at both ends. Hereafter, without loss of generality, we assume that the current of the generators is given, i.e., we work with *current excitation*.

As mentioned in the introduction, the wire consists of insulated strands that are connected with each other at the ends of the wire. Thus, the following conditions are fulfilled for the arrangement:

- The longitudinal period of the wire is much larger than the wire diameter.
- The length of the wire is many times greater than the longitudinal period.
- The leads of the generator are arranged such that the effect of their magnetic field on the current distribution in the wire can be neglected.

In this case, we assume that the losses of the wire can be calculated with good approximation based on a single representative cross-sectional current distribution. This cross-section is taken at a sufficient distance from the ends where the leads do not cause any distortion in the current distribution. The current distribution can be determined from a two-dimensional boundary value problem on the  $\Omega$  domain. We need to formulate 2D boundary value problems that consistently take into account both the

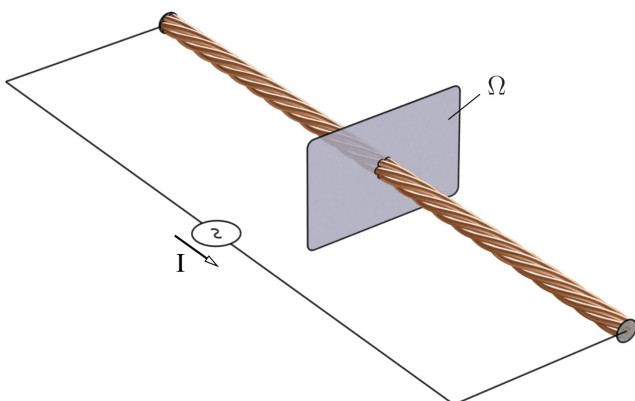


Fig. 1 Litz wire with current excitation

twisting-braiding and circuit environment constraints and are suitable for calculating the wire losses.

### 2.1 Maxwell equations and potential formulations

Due to the typical frequency and size range, the electromagnetic field and current distribution in the conductors can be calculated using the magnetoquasi-static (MQS) approximation of Maxwell's equations [10, 11]. The basic equations in the frequency domain are:

$$\nabla \times \mathbf{H} = \mathbf{J}, \quad (1)$$

$$\nabla \times \mathbf{E} = -j\omega \mathbf{B}, \quad (2)$$

$$\nabla \times \mathbf{B} = 0, \quad (3)$$

where  $\mathbf{E}$ ,  $\mathbf{B}$ ,  $\mathbf{H}$  and  $\mathbf{J}$  are the complex amplitudes of the electric field strength, magnetic induction, magnetic field strength, and current density vector, respectively,  $\omega$  is the angular frequency, and  $j$  is the imaginary unit. The constitutive equations are:

$$\mathbf{B} = \mu \mathbf{H}, \quad (4)$$

$$\mathbf{J} = \sigma \mathbf{E}, \quad (5)$$

where  $\mu$  and  $\sigma$  are the permeability and specific conductivity of the medium. In solving the problem, we use the  $\mathbf{A} - V$ ,  $\mathbf{A}$  method commonly used in eddy current problems, that is:

$$\mathbf{B} = \nabla \times \mathbf{A}, \quad (6)$$

$$\mathbf{E} = -j\omega \mathbf{A} - \nabla V. \quad (7)$$

Furthermore, the divergence of  $\mathbf{A}$  is freely chosen, which is conventionally constrained by the Coulomb gauge in solving MQS problems:

$$\nabla \times \mathbf{A} = 0. \quad (8)$$

Taking into Ampere's law (Eqs. (1) and (5)) takes the following form, where  $\nu = 1/\mu$  is the so-called reluctivity:

$$\nabla \times \nu \nabla \times \mathbf{A} + j\omega \sigma \mathbf{A} = -\sigma \nabla V. \quad (9)$$

Equation (10) reduces to the following in an insulating medium:

$$\nabla \times \nu \nabla \times \mathbf{A} = 0. \quad (10)$$

Furthermore, the scalar Laplace equation for the electric scalar potential  $V$  can be derived:

$$\nabla^2 V = 0. \quad (11)$$

## 2.2 Continuity

The partial differential equations of Eqs. (9)–(11) should be supplemented with known continuity conditions at the boundaries of the medium:

$$[\mathbf{n} \times \mathbf{B}] = 0, [\mathbf{n} \times \mathbf{H}] = 0, [\mathbf{n} \times \mathbf{E}] = 0, \quad (12)$$

where  $\mathbf{n}$  is the surface normal vector and  $[\ ]$  denotes the jump of the enclosed quantity at the medium boundary. Specifically, at the conductor-insulator interface, the following conditions must be satisfied:

$$\mathbf{n} \times \mathbf{J} = 0. \quad (13)$$

In the case of a closed model domain, the necessary boundary conditions are added to the above. The special cases of boundary and interface conditions, as well as their formulation with potentials, will be given in the two-dimensional boundary value problem.

## 2.3 Model domain

Let us first consider not twisted, parallel wire cable. We do not make any assumptions about the cross-section or arrangement of the wires. (see Fig. 2) Assume that the arrangement has quasi-translational symmetry in the  $z$  direction. Let its length be denoted by  $l$ . The two-dimensional model domain  $\Omega$  taken in the transverse plane has a boundary  $\Gamma$  (see Fig. 2). The model domain can be decomposed into the disjoint  $\Omega_i (i = 1 \dots n)$  conductor and the  $\Omega_0$  non-conductor (e.g., air) domains surrounding them. The value of  $\mathbf{n} \times \mathbf{B}$  is given on the  $\Gamma_B$  boundary segment, while  $\mathbf{n} \times \mathbf{H}$  is given on the  $\Gamma_H$  boundary segment.

## 2.4 Boundary value problem

Assuming that a purely  $z$ -directional current flows in the cross-section of the conductors, the magnetic induction vector is purely transverse except near the ends. Based on the Coulomb gauge and the expression for the potentials in terms of Eqs. (6) and (7), and because of the Coulomb gauge Eq. (8) it can be shown that  $\mathbf{A}$  is also purely  $z$ -directional and, like  $\mathbf{J}$  and  $\mathbf{B}$ , independent of the longitudinal coordinate, that is,  $z$ -invariant, which reads as:

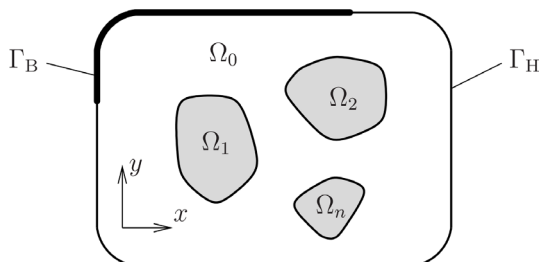


Fig. 2 Model domain of untwisted, parallel wires

$$\begin{aligned} \mathbf{J} = \mathbf{e}_z J_z(x, y) &\Rightarrow \mathbf{B} = \mathbf{e}_x B_x(x, y) \\ + \mathbf{e}_y B_y(x, y) &\Rightarrow \mathbf{A} = \mathbf{e}_z A_z(x, y). \end{aligned} \quad (14)$$

On the other hand, the scalar potential  $V$ , which is only defined in the conductors, is not  $z$ -invariant, as can be easily seen by comparing the aforementioned property of  $\mathbf{J}$ , the differential Ohm's law (Eq. (5)), and the expression of  $\mathbf{E}$  in Eq. (6). However, it follows from these that the gradient of  $V$  is  $z$ -directed and constant within each conductor:

$$\nabla V = \mathbf{e}_z \frac{\partial V}{\partial z}, \quad \left. \frac{\partial V}{\partial z} \right|_{\Omega_i} = e_i = \text{const.} \quad i = 1 \dots n. \quad (15)$$

The continuity of the spatial components in Eq. (12) can be represented by the following conditions:

$$[\mathbf{n} \times \mathbf{B}] = 0 \Leftrightarrow [A_z] = 0, \quad (16)$$

$$[\mathbf{n} \times \mathbf{H}] = 0 \Leftrightarrow [\mathbf{n} \times \nu \nabla_T A_z] = 0. \quad (17)$$

These conditions are satisfied by default in the conventional implementation of the finite element method. The continuity of the tangential component of the electric field is not considered at the conductor-insulator interface.

Substituting these into Eqs. (9) and (10) and supplementing with the boundary conditions, we obtain the following two-dimensional scalar boundary value problem:

$$\Omega_0 : \nabla_T \times \nu \nabla_T A_z = 0, \quad (18)$$

$$\Omega_i (i = 1 \dots n) : \nabla_T \times \nu \nabla_T A_z + j\omega\sigma A_z = -\sigma e_i, \quad (19)$$

$$\Gamma_B : A_z = A_0, \quad (20)$$

$$\Gamma_H : \mathbf{n} \times \nu \nabla_T A_z = H_0. \quad (21)$$

The field intensities can be expressed from the solution  $A_z(x, y)$ :

$$\Omega : \mathbf{B} = \frac{\partial A_z}{\partial y} \mathbf{e}_x - \frac{\partial A_z}{\partial x} \mathbf{e}_y, \quad (22)$$

$$\Omega_i (i = 1 \dots n) : \mathbf{E} = -j\omega A_z \mathbf{e}_i. \quad (23)$$

## 2.5 Circuit laws

The solution of the boundary value problem (Eqs. (18)–(21)) is not unique, as it contains  $n$  unknowns – which have same dimension as the electric field – and can only be determined with knowledge of the entire 3D environment. On the other hand, there are  $n$  base solutions that can be calculated for the  $e_i$  parameters as excitations, of which

linear combination can generate any field distribution that exists on the given cross-section [12].

To determine the parameters  $e_j$ , let us formulate voltage constraints. Consider the  $\Omega_j$  and  $\Omega_k$  conductive regions and take two arbitrary points  $P(x_j, y_j)$  and  $P(x_k, y_k)$  within them. Form a rectangular loop from the straight line segments passing through the points in the  $z$ -direction, which extends over the entire length  $l$  of the arrangement and connect them at their respective ends (see Fig. 3).

The Faraday's law of induction for this loop:

$$\oint \mathbf{E} \times d\mathbf{l} = -j\omega\Psi = -j\omega \oint \mathbf{A} \times d\mathbf{l}, \quad (24)$$

where  $\Psi$  is the magnetic flux of the loop. By performing the integrals section by section and using the expression of the electric field in terms of Eq. (23), Eq. (25) can be written:

$$\begin{aligned} & l[-j\omega A_z(x_j, y_j) - e_j] + U_a \\ & - l[-j\omega A_z(x_k, y_k) - e_k] - U_b \\ & = -j\omega [A_z(x_j, y_j)l - A_z(x_k, y_k)l], \end{aligned} \quad (25)$$

where  $U_a$  and  $U_b$  represent the voltage applied between the conductors at the two ends of the configuration; since the wire ends are in metallic contact, we consider these to be zero. The integral of the vector potential precisely compensates for both sides of the equation, giving us the following result:

$$e_j l = e_k l. \quad (26)$$

We intentionally do not simplify with the length  $l$  (see later) since the length of the twisted wires may differ. In this way,  $n - 1$  independent equations can be written for the  $n$  conductors, but it is more practical to use the following form consisting of  $n$  equations:

$$e_i l = U, \quad i = 1 \dots n. \quad (27)$$

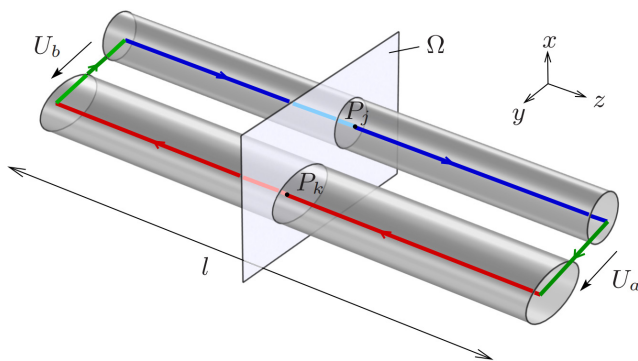


Fig. 3 Faraday's law on untwisted wires

Since we introduced a new unknown variable  $U$ , we need one further equation. This is the current constraint. The expression for current density in the  $k$ -th conductor is:

$$\Omega_k : J_z = \sigma_k (-j\omega A_z - e_k). \quad (28)$$

This leads to the complex amplitude of the current in this conductor:

$$I_k = \int_{\Omega_k} J_z d\Omega. \quad (29)$$

In the wire strands, the sum of the currents must be equal to the excitation current, which is considered given in the problem definition:

$$I = \sum_{k=1}^n I_k. \quad (30)$$

## 2.6 Effect of stranding and twisting

The purpose of twisting or braiding the insulated conductive wires in a litz wire is to make them electromagnetically equivalent to the wire ends, ensuring uniform distribution of current among the wires. This not only optimizes the utilization of wire cross-section but also minimizes losses. In the two-dimensional model, this equivalence must be appropriately taken into account.

Let us consider the schematic two-dimensional model domain shown in Fig. 4, in which the domains of the strands considered equivalent are grouped and labeled with double indices:  $\Omega_{gs}$  strands for the  $s$ -th ( $s = 1 \dots n_g$ ) strand of the  $g$ -th group ( $g = 1 \dots m$ ). Thus, a group consists of  $n_g$  strands. On the left side of Fig. 4, we can see a twisted wire consisting of seven strands, of which the six peripheral strands can be considered equivalent, but the central one cannot because it remains stationary during the twisting process. On the right side, there is a wire woven from six strands with a square cross-section, in which every strand is equivalent.

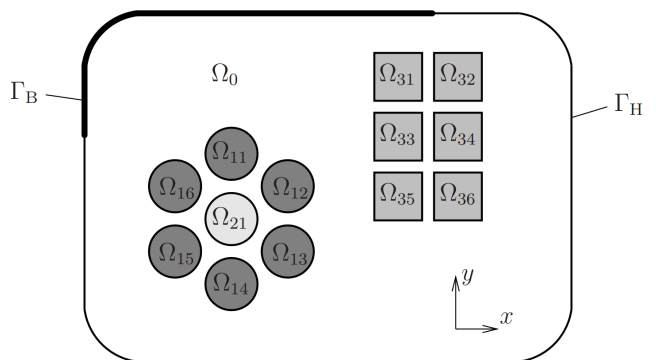


Fig. 4 Modell domain of twisted cables

One obvious condition for equivalence is that all strands within a group carry the same current:

$$\int_{\Omega_{gs}} J_z d\Omega = I_g \quad s = 1 \dots n_g. \quad (31)$$

The other condition concerns the voltage drop, expressing that the wires make contact at the ends of the wire. Similar to before, we use Faraday's law of induction, but its formulation requires a certain approximation, which is illustrated below using the example of a seven-wire twisted litz wire on Fig. 5.

Let the closed loop (used to write the induction law – see Fig. 5) be written along the axis of one peripheral strand (red line), and return along the axis of the central strand (blue line), as shown on the left side of Fig. 5. This path needs to be mapped onto a two-dimensional problem that assumes translational symmetry, meaning essentially parallel conductor strands. This obviously poses no problem at the central strand. For the twisted strand, an obvious solution is to approximate the helix with straight segments in the  $z$ -direction by systematically switching between peripheral conductor strands in an untwisted cable. In three dimensions, this can be imagined as the stepped curve shape on the right side of Fig. 5, but it is important to note that the segments corresponding to the switches (dashed black lines) do not form part of the integration path.

In general, we can state that the integral path mapped onto a 2D problem statistically passes through all conductor domains belonging to the group in equal length. The electric field is integrated over such a path:

$$\int \mathbf{E} \times d\mathbf{l} \approx \sum_{s=1}^{n_g} \frac{\alpha_g l}{n_g} (-j\omega A_z - e_{gs}). \quad (32)$$

In Eq. (32),  $\alpha_g$  is the so-called length correction factor (due to the twisting of the conductors, the length of the twisted conductors is generally longer than the actual length of the cable), and  $e_{gs}$  is the constant parameter of the

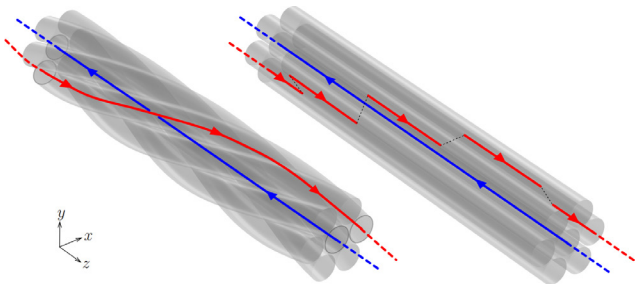


Fig. 5 Loop for writing Faraday's law on twisted wires

PDE using the above introduced two-index notation. It is useful to introduce the averaged voltage drop for the group:

$$U_g = \frac{\alpha_g l}{n_g} \sum_{s=1}^{n_g} e_{gs}. \quad (33)$$

The excitation current specified in the problem definition is the sum of the group currents:

$$\sum_{g=1}^m n_g I_g = I. \quad (34)$$

The system of equations to be solved:

$$\left. \begin{aligned} \nabla_T \times \nu \nabla_T A_z &= \Omega_0 \\ \nabla_T \times \nu \nabla_T A_z + j\omega \sigma A_z &= -\sigma e_i \\ A_z &= A_0 \\ \mathbf{n} \times \nu \nabla_T A_z &= H_0 \end{aligned} \right\} \begin{array}{l} \Omega_0 \\ \nabla \Omega_{gs} \\ \Gamma_B \\ \Gamma_H \end{array} \text{BVP}, \quad (35)$$

$$\left. \begin{aligned} \frac{\alpha_g l}{n_g} \sum_{s=1}^{n_g} e_{gs} &= U_g \quad \forall g \\ \int_{\Omega_{gs}} J_z d\Omega &= I_g \quad \forall s, g \end{aligned} \right\} \text{Stranding and twisting}, \quad (36)$$

$$\left. \begin{aligned} U_g &= U \quad \forall g \\ \sum_{g=1}^m n_g I_g &= I \end{aligned} \right\} \text{Circuit laws}. \quad (37)$$

From this,  $A_z(x, y)$ ,  $e_{gs}$ ,  $U_g$ ,  $I_g$  and  $U$  quantities can be determined given  $I$ ,  $A_0$  and  $H_0$  (the latter two often being 0).

## 2.7 Losses, resistance

After solving the partial differential equation, the total power density can be obtained by integrating the volume power density (that is expressed by squared magnitude of  $J_z$ ) current density over the representative cross section, from which the so-called high-frequency resistance can be calculated:

$$P = \frac{1}{2} l \sum_{g=1}^m \alpha_g \sum_{s=1}^{n_g} \int_{\Omega_{gs}} \frac{|J_z|^2}{\sigma_{gs}} d\Omega, \quad (38)$$

$$R = \frac{2P}{|I|^2}. \quad (39)$$

The total wire resistance reads as:

$$R = \frac{1}{|I|^2} l \sum_{g=1}^m \alpha_g \sum_{s=1}^{n_g} \int_{\Omega_{gs}} \sigma | -j\omega A_z - e_{gs} |^2 d\Omega. \quad (40)$$

## 3 Examples

We carried out the test calculations on three wires shown 0 in Fig. 6, which are named  $A$ ,  $B$  and  $C$  wire types. All of

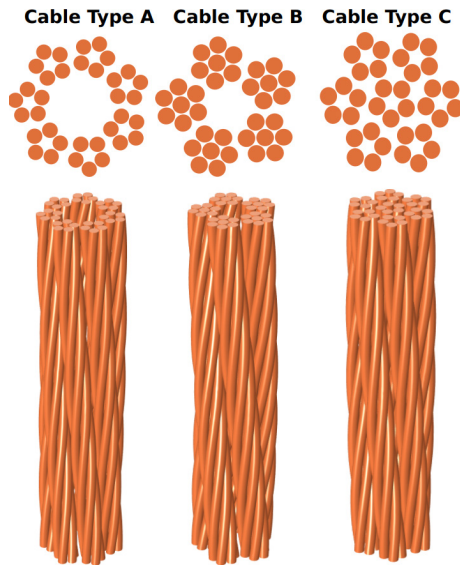


Fig. 6 Three different bundle structures with equal conductor cross section

them consist of 35 elementary conductor wires, so they have the same cross-section of copper, but their structure is different. The diameter of an elementary conductor wire is 0.24 mm for each cable, and the enamel coating – whose magnetic properties are the same as that of air, so we treat it in the model the same way as air – has a thickness of 7 μm.

In the wires, the elementary wires are organized into bundles, and the structure of these bundles forms the full wire cross-section.

Let  $s$  denote the number of elementary wires and  $g$  the number of groups in the bundle. In the higher-order, cable-level structure, let  $S$  be the number of elementary bundles and  $G$  be the number of groups in the cable. Formally, the structure of the cables is described by the Table 1.

The modeling of the three cables was performed in both two- and three-dimensions, and the obtained results and computation times were compared. The two-dimensional model was created using MATLAB PDE Toolbox [13], as it is well-configurable, flexible, and can utilize all MATLAB functions during preparation and post-processing. The two-dimensional calculations were validated against the three-dimensional calculations, which was justified since the aim of the work was to reduce the three-dimensional calculations to two dimensions. The three-dimensional

Table 1 Formal hierarch of cables

Cable type	$g$	$s$	$G$	$S$
A	1	5	1	7
B	2	1 + 6	1	5
C	1	5	2	1 + 6

model of the cables was created by colleagues from the department using Comsol Multiphysics.

### 3.1 Resistance per unit length as a function of frequency

On Fig. 7 the increase of resistance per unit length of the cables with increasing frequency can be seen. The frequency range was 50–300 kHz. There is almost perfect agreement between the two- and three-dimensional results. It is noticeable that although the examined constructions have the same copper cross-section, their frequency-resistance characteristics are quite different. These characteristics start from the value of the cable's DC resistance, given by:

$$r = \frac{1}{\sigma A_{sum}} \alpha = 10.6629 \frac{m\Omega}{m} \quad (41)$$

In Eq. (41)  $\alpha$  is the length correction factor discussed earlier. The phenomenon causing the difference in characteristics appears at higher frequencies. The value of penetration depth due to skin effect remains – even at the highest frequency of  $f = 300$  kHz:

$$\delta = \sqrt{\frac{2}{2\pi f \sigma \mu}} = 0.1187 \text{ mm.} \quad (42)$$

With this ratio between the penetration depth and the radius of the elementary conductor, the current distribution  $J$  within the cross section is approximately uniform. Therefore, its effect is not significant, even at the highest tested frequency, and it would not justify the difference between the wire constructions. The results of the 2D and 3D modelling methods show good agreement. The differences between the results are discussed in Section 3.2.

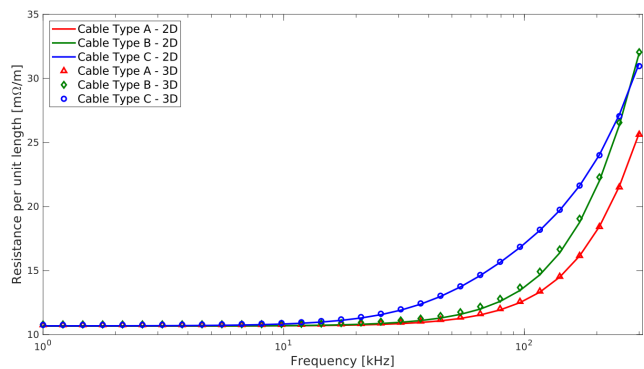


Fig. 7 Resistance per unit length as a function of frequency

### 3.2 Current of individual strands as a function of frequency

In Fig. 8 we can see the current of an individual wire in the central bundle and one of the peripheral bundles of a selected C-type cable.

It can be observed that while the amplitude of the current in the central bundle does not decrease significantly, its phase starts to increase sharply. Although the total current in the cable is still prescribed, the amplitude of the current in the peripheral bundle increases significantly, but their phase decreases only slightly. This is explained by the bundle-level skin effect [14]. This also causes the difference in resistance-frequency characteristics of cables.

### 3.3 Examination of current distribution at fixed frequency

In Section 3.3, we examine the instantaneous value and magnitude of the current distribution of cable C. On Fig. 9 the instantaneous value of the current peak can be seen at

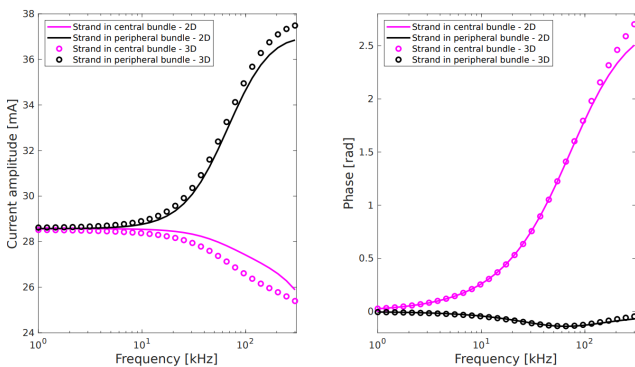


Fig. 8 Elementary wire currents as a function of frequency

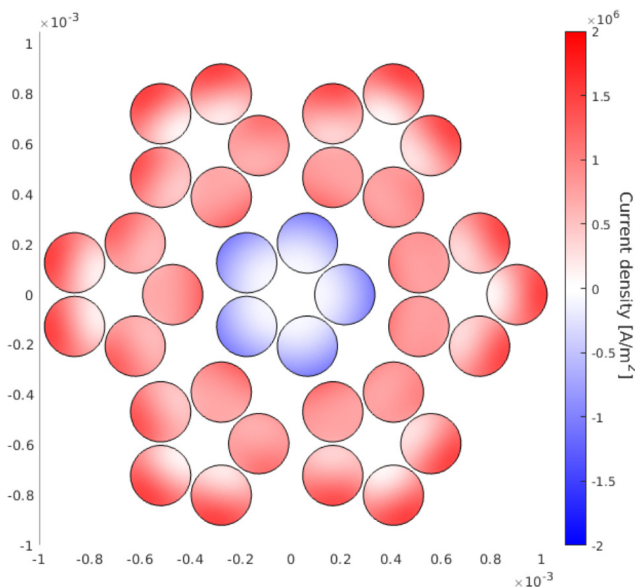


Fig. 9 Current density at fixed frequency ( $f = 300$  kHz;  $t = 0$  s)

$f = 300$  kHz frequency. As can be observed on Fig. 9, while the middle bundle has negative current flow, the peripheral bundles have positive current flow. This effect also increases the resistance per unit length of the cable.

The validation of the two-dimensional model can be performed in more detail by examining the distribution of the magnitude of current density. In Fig. 10 the magnitude of current on the C-type cable at  $f = 300$  kHz frequency is shown (the colorbar is the same in the two figures). The two- and three-dimensional models show good agreement in this more detailed comparison as well.

### 3.4 Comparison of computation time

To generate the curves shown above, we calculated the resistance of the cable per unit length at 30 points. The cross-sectional model (2D) required 184 seconds to

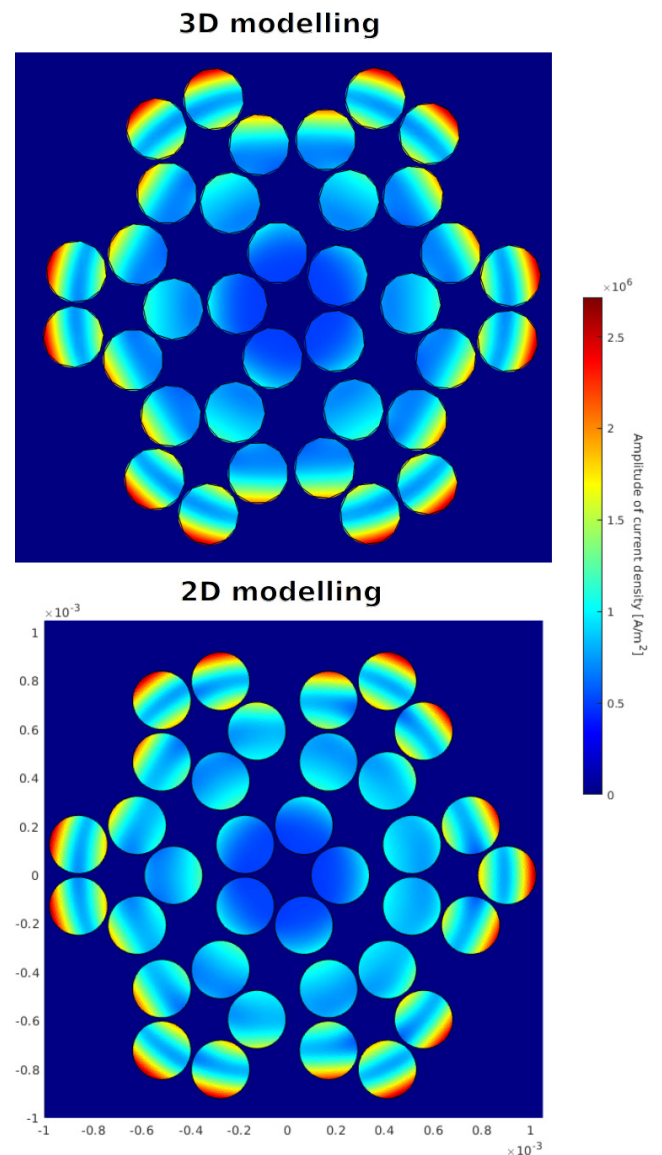


Fig. 10 Amplitude of current density ( $f = 300$  kHz)

run, whereas the three-dimensional cable models took more than 10 hours to run.

#### 4 Summary

In this paper, after theoretical derivations related to the modeling of multi-conductor cables, a framework for the numerical simulation by means finite element method coupled with current and voltage constraints was presented. Three cable constructions were shown and it was also presented, how their resistance per unit length varies with frequency and the effects that contribute to the losses of twisted conductors. The two-dimensional model calculations were validated with three-dimensional model calculations. The following conclusions can be drawn:

- The developed two-dimensional cross-sectional models can be easily created and adapted to various wire structures. They lead to a consistent equation system, which can be solved in one step, significantly reducing the runtime compared to three-dimensional modeling.

#### References

- [1] Guillod, T., Huber, J., Krismer, F., Kolar, J. W. "Litz wire losses: Effects of twisting imperfections", In: 2017 IEEE 18th Workshop on Control and Modeling for Power Electronics (COMPEL), Stanford, CA, USA, 2017, pp. 1–8. ISBN 978-1-5090-5327-8  
<https://doi.org/10.1109/COMPEL.2017.8013327>
- [2] Panchal, J., Lehtikoinen, A., Rasilo, P. "Efficient finite element modelling of litz wires in toroidal inductors", IET Power Electronics, 14(16), pp. 2610–2619, 2021.  
<https://doi.org/10.1049/pe1.12206>
- [3] Sullivan, C. R. "Optimal choice for number of strands in a litz-wire transformer winding", IEEE Transactions on Power Electronics, 14(2), pp. 283–291, 1999.  
<https://doi.org/10.1109/63.750181>
- [4] Hiruma, S., Otomo, Y., Igarashi, H. "Eddy Current Analysis of Litz Wire Using Homogenization-Based FEM in Conjunction With Integral Equation", IEEE Transactions on Magnetics, 54(3), 7001404, 2018.  
<https://doi.org/10.1109/TMAG.2017.2772335>
- [5] Roszkopf, A., Schuster, S., Endruschat, A., Bär, E. "Influence of varying bundle structures on power electronic systems simulated by a coupled approach of FEM and PEEC", In: 2016 IEEE Conference on Electromagnetic Field Computation (CEFC), Miami, FL, USA, 2016, pp. 1–1. ISBN 978-1-5090-1033-2  
<https://doi.org/10.1109/CEFC.2016.7816288>
- [6] Gyselinck, J., Dular, P. "Frequency-domain homogenization of bundles of wires in 2-D magnetodynamic FE calculations", IEEE Transactions on Magnetics, 41(5), pp. 1416–1419, 2005.  
<https://doi.org/10.1109/TMAG.2005.844534>
- [7] Konrad, A., Chari, M., Csendes, Z. "New finite element techniques for skin effect problems", IEEE Transactions on Magnetics, 18(2), pp. 450–455, 1982.  
<https://doi.org/10.1109/TMAG.1982.1061859>
- [8] Preis, K. "A contribution to eddy current calculations in plane and axisymmetric multiconductor systems", IEEE Transactions on Magnetics, 19(6), pp. 2397–2400, 1983.  
<https://doi.org/10.1109/TMAG.1983.1062876>
- [9] Fejérvári, L., Bilicz, S., Gyimóthy, S., Pávó, J., Varga, G., Várallyay, Z., Yamada, Y., Shimura, T., Orito, H., Azuma, Y. "Electromagnetic modeling of coils made of twisted litz wire by combining finite element simulation and circuit laws", International Journal of Applied Electromagnetics and Mechanics, 70(1), pp. 21–31, 2022.  
<https://doi.org/10.3233/JAE-210205>
- [10] Simonyi, K., Zombory, L. "Elméleti villamosságatan" (Theoretical Electromagnetics), Műszaki Könyvkiadó, 2000. ISBN 963-16-3058-7 (in Hungarian)
- [11] Biro, O., Richter, K. R. "CAD in Electromagnetism", Advances in Electronics and Electron Physics, 82, pp. 1–96, 1991.  
[https://doi.org/10.1016/S0065-2539\(08\)60911-7](https://doi.org/10.1016/S0065-2539(08)60911-7)
- [12] Bossavit, A. "Eddy currents in dimension 2: Voltage drops", In: 10th International Symposium on Theoretical Electrical Engineering, Magdeburg, Germany, 1999, pp. 103–107.
- [13] Mathworks "MATLAB PDE Toolbox (R2022b)," [computer program] Available at: <https://mathworks.com> [Accessed: 03 July 2022]
- [14] Gyimóthy, S., Kaya, S., Obara, D., Shimada, M., Masuda, M., Bilicz, S., Pávó, J., Varga, G. "Loss Computation Method for Litz Cables With Emphasis on Bundle-Level Skin Effect", IEEE Transactions on Magnetics, 55(6), 6300304, 2019.  
<https://doi.org/10.1109/TMAG.2019.2890969>

The method can be extended to multi-level layouts. An interesting further extension is to apply magnetically coated elementary conductor wires to reduce wire losses, which result in lower losses due to optimal distribution of the magnetic field. The presented method can be extended to such wires.

- We observe good agreement between the results of the two modeling methods not only in the frequency dependence of the alternating current resistance but also in more detailed results, such as the current density distribution at higher frequencies.
- The difference of the resistance-frequency characteristics can partially be explained by the different strength of this bundle level skin effect in each type of cable structure, although the proximity effect may also show dependence on the arrangement of the strands.